

Backward Renormalization Priors and the Cortical Source Localization Problem with EEG or MEG

Leonardo S Barbosa^{1,2} and Nestor Caticha¹

¹*Instituto de Física, Universidade de São Paulo*

²*Laboratoire de Science Cognitive et Psycholinguistique, Ecole Normale Supérieure*

(Dated February 10, 2015)

Abstract We study source localization from high dimensional M/EEG data by extending a multiscale method based on Entropic inference devised to increase the spatial resolution of inverse problems . This method is used to construct informative prior distributions in a manner inspired in the context of fMRI (Amaral et al 2004 [1]) . We construct a set of renormalized lattices that approximate the cortex region where the source activity is located and address the related problem of defining the relevant variables in a coarser scale representation of the cortex. The priors can be used in conjunction with other Bayesian methods such as the Variational Bayes method (VB, Sato et al 2004 [22]). The central point of the algorithm is that it uses a posterior obtained at a coarse scale to induce a prior at the next finer scale stage of the problem. We present results which suggest, on simulated data, that this way of including prior information is a useful aid for the source location problem. This is judged by the rate and magnitude of errors in source localization. Better convergence times are also achieved. We also present results on public data collected during a face recognition task.

Keywords: Maximum Entropy, priors, cortical source localization, EEG, MEG, Bayesian algorithms, inverse problems

1 Introduction

Designing improved methods of inference by updating probabilities as new information is acquired, depends partly on the development of ideas of how to incorporate prior information. In this paper we concentrate on the construction of prior distributions for the localization of cortical dipole sources in EEG or MEG high resolution experiments. Several groups have presented very encouraging results with respect to source localization (for a review see [21]). After data acquisition, the source localization analysis problem is divided into three essentially separate problems: first, construction of the prior; second, of the likelihood or model and third, of the algorithm to extract the information from the resulting posterior. Several such information extraction algorithms have been systematically analyzed by Wipf and Nagarajan [24] in a useful unification that simplifies the literature, since different Bayesian approaches differ only in the available information. Sato *et al* [22] have tackled the construction of empirical priors. Our approach, which can also focus on an empirical prior is based on a previously introduced multiscale-prior method [4] which formalized ideas applied in the context of fMRI by [1], [2]. It relies on the maximum entropy (ME) method to transfer information gained at a coarse scale to start inference at a finer scale.

Advances by Dale and Sereno [5] permitted the inclusion of information from structural MRI to construct a Green's function that is specific to the subject under study. This can be used in a Bayesian approach as such additional information can be incorporated in the construction of the model and therefore of the likelihood. Once a posterior distribution is constructed, it still remains to choose an appropriate numerical algorithm in order to extract relevant information in the form of expected values or MAP estimates. Sato *et al* [22] use the Automatic Relevance Determination approach of Neal [15] through the Variational Bayes (VB) approximation, (see also [3]) while Nummema *et al.* [16] analyzed essentially the same mathematical structure using both VB and Monte Carlo methods. A schematic description of the VB method we employ is given in section 2.1.

In sections 2.2 and 2.3 we describe the central part of this work, the method of backward renormalization priors based on entropic inference. We show how to use information obtained at a coarse renormalized scale to improve the starting point on a finer scale. This can be iterated up from a very coarse description of the system to the finest scale. The presentation is very general and the particular form of the set of renormalized lattices depends on the application at hand.

Validation of the method appears in section 3 using simulated data sets. After calculating the forward model with a set of known dipole sources, we assess the results comparing the performance of the source localization of 2 dipoles at random positions and intensities using both the original VB method and the multiscale approach. This is done comparing the distance between the localized dipole (or first N strongest dipoles) and the *real* one (used to generate the simulated data), and also the sensitivity of both algorithms (ROC curves) when the noise is increased. Finally, we applied our method to the problem of source localization of a face/mask paradigm in the data available at <http://www.fil.ion.ucl.ac.uk/spm/data/> (SPM - Wellcome Trust Centre for Neuroimaging). A discussion and conclusions appear in the final section.

2 Methods

Since our contribution lies in the proposed method, this is the central part of the paper. But first we describe the inverse problem in section 2.1. In this part we don't make any advances and follow the work of Sato *et al.* [22]). Then, in 2.2 we discuss the central part of our contribution, the multiscale approach to the prior distribution.

2.1 The forward and inverse problems: from cortical sources to M/EEG data and back

We follow Sato [22]) using a linear model that has been discussed by [17], [8] [13], [14] [18] (see also [23]). We denote by V the electric potential at the scalp surface, by J the density of dipole sources that give rise to those potentials and G the Green function that describes the electromagnetic medium. It represents the macroscopic physiological and geometrical details of the head known in this area as the *Lead Field*.

Measurements are subject to noise ξ that has been supposed to be gaussian and independent of space and time, so that for data V and dipole sources density J the model is

$$V = GJ + \xi. \quad (1)$$

For M sensors, T the length of the time series of measurements, N the number of sites of the lattice where the dipoles live, the dimensions of the matrices V, J, G and ξ are respectively $M \times T, N \times T, N \times M$ and $M \times T$. Bayes theorem leads to

$$P(J|VI) = \frac{P_0(J|I)P(V|JI)}{P(V|I)}. \quad (2)$$

The method that we follow is essentially the variational Bayes used by Sato *et al.* with a twist. In their method, the prior distribution of the dipole density $P(J_d) = P(\{J_d(r^d(i))\})$ is parametrized by a set of parameters $\alpha_d = \{\alpha_d(i)\}$ where Λ_d is the lattice of positions $r^d(i)$ used to represent the cortex where the dipoles live. $\alpha_d(i)$ is the inverse of the variance of the zero mean gaussian also called the precision, used as prior for the dipole density vector amplitude $J_d(r^d(i))$ at each site $i \in \Lambda_d$. The direction of each $J_d(r^d(i))$ vector is fixed and normal to the surface representing the cortex at that point. Incomplete knowledge of α_d prompts the use of hyperpriors for each individual $\alpha_d(i)$. It is reasonable, as they do, to use a set of Gamma hyperprior distributions for the set of $\alpha_d(i)$. Integrating the gaussian priors over the Gamma distributed $\alpha_d(i)$ leads to t-student distributions. So that at each site, the distributions of the density belong to the family given by

$$\begin{aligned} P(J|\bar{\alpha}, \gamma) &= \int_0^\infty \frac{\alpha^{1/2}}{\sqrt{2\pi}} e^{-\frac{\alpha j^2}{2}} \Gamma(\alpha|\hat{\alpha}, \hat{\gamma}) d\alpha \\ &= \sqrt{\frac{\bar{\alpha}}{2\pi\gamma}} \frac{\Gamma(\gamma + \frac{1}{2})}{\Gamma(\gamma)} \frac{1}{\left[1 + \frac{j^2 \bar{\alpha}}{2\gamma}\right]^{\gamma+1/2}}. \end{aligned} \quad (3)$$

Call collectively the set of hyperparameters of the Gammas θ_d^0 . The inclusion of the data read from the electrodes, V , by the Variational Bayes method, leads to a dynamics of the hyperparameters of the gammas, which converges to a final value θ_d^f . Their method can be succinctly described by the mapping

$$\theta_d^0 = (\hat{\alpha}_d^0, \gamma_d^0) \xrightarrow{\text{Variational Bayes}} \theta_d^f = (\hat{\alpha}_d^f, \gamma_d^f) \quad (4)$$

Their starting point is that every $\theta_d^0(r^d(i)) \in \theta_0^d$ is the same, i.e a prior of the dipole density spatially invariant over the cortex.

Our contribution consists of considering a different choice of the prior distributions. For this we use the theory of backward [4] renormalization priors, which are inspired in the multigrid prior approach used by [1] to study fMRI. By using entropic inference, we can use the posterior in a coarse scale to generate an informed prior in the next finer scale.

2.2 The Multiscale problem

The relevant variables are the dipoles densities J and the electric potential (or magnetic fluxes) to be measured at the electrodes. The space where the variables live is a representation of the cortex obtained from structural magnetic resonance data using Free Surfer image analysis suite, which is documented and freely available for download online (<http://surfer.nmr.mgh.harvard.edu/> - [6] [7]). This representation can be done at different levels of resolution, so that we define a set of renormalized lattices $\{\Lambda_d\}_{d=0,\dots,D}$. Each lattice is composed by sites $r^d(i) \in \Lambda_d$ with $i = 1, \dots, |\Lambda_d|$. The particular form of how a coarser or renormalized lattice Λ_{d-1} is obtained from the previous Λ_d depends on the particular type of problem. For the problem at hand of EEG dipole sources, the first lattice Λ_0 was generated by introducing an icosahedron in the spherical surface (Figure 1) obtained by inflating a brain hemisphere. Deflating the spheres results in a first lattice with 40 faces. Next, to generate the finer scales lattices $\Lambda_1, \dots, \Lambda_D$, each triangular face of the inflated brain was into 4 triangles. More details about the position of dipoles in each face are given in section 3.1.

At each scale d there is a set of dipole density amplitudes, collectively denoted $J_d = \{J_d(r^d(i))\}$. We denote the integration measure over the set of $|\Lambda_d|$ variables by dJ_d .

Consider just two consecutive scales, a coarse one $d - 1$ and the higher resolution d . Suppose we have solved the case at the $d - 1$ level and now we want to solve the problem at scale d . This will give a map to be iterated from the coarsest to the finest scale. The method to be used follows the simpler case of discrete variables presented in [4] is the maximum entropy (ME), and the aim is to obtain a distribution $P(J_d, J_{d-1}, V)$ from a prior distribution $Q(J_d, J_{d-1}, V)$. The method of choice is the ME because (i) when constraints are imposed and the prior already satisfies the constraints ME will result in a posterior equal to the prior and (ii) when the results of a measurement are considered as constraints, ME gives the same results as Bayes [9]. Bayesian usual update can be thought of as a special case of Maximum Entropy where the constraints arise from the data.

To show (i) we perform a simple Maximum Entropy exercise: Consider a variable X that takes values x and that $Q(x)$ represents our prior state of knowledge. New information is obtained, e.g that the expected value $\langle f(x) \rangle$ is known to have a particular value: $\langle f(x) \rangle = E$. The update from $Q(x)$ to $P(x)$ is done by maximizing

$$S[P||Q] = - \int P(x) \log \frac{P(x)}{Q(x)} dx + \lambda \left(\int f(x) dx - E \right) + \lambda_0 \left(\int P(x) dx - 1 \right) \quad (5)$$

The result, after satisfying normalization is the Boltzmann-Gibbs probability density $P(x) = Q(x) \frac{\exp \lambda f(x)}{Z(\lambda)}$, with λ to be chosen to satisfy $\langle f(x) \rangle_p = E$. What is the value of λ if $\langle f(x) \rangle_Q = E$, if the prior already satisfied the constraint? It is simple to see that $\lambda = 0$ and $Z(\lambda) = 1$, so the reuse of old data in the form of constraints, again and again doesn't change the density $Q(x)$ that already satisfies the constraint. While this sounds trivial, it will be useful since data in Bayes updates can be written as constraints for Maximum Entropy.

To prove condition (ii) we follow [9]. Consider the problem where a distribution $P(\theta)$ has to be obtained, first, from the knowledge that a measurement of X has yielded a datum

x' ; second, that prior to the inclusion of such information our knowledge of θ is codified by a distribution $Q(\theta)$ and third, that the relation between X and Θ is codified by a likelihood $Q(x|\theta)$. Thus we have to consider $P(x, \theta)$ subject to constraints $\int d\theta P(x, \theta) = P(x) = \delta(x - x')$. This is not a single constraint, i.e. instead of a single Lagrange multiplier, we have to consider a function $\lambda(x)$ and maximize

$$S[P||Q] = - \int P(x, \theta) \log \frac{P(x, \theta)}{Q(x, \theta)} dx d\theta + \int \lambda(x) \left(\int d\theta P(x, \theta) - \delta(x - x') \right) dx + \lambda_0 \left(\int P(x) dx - 1 \right). \quad (6)$$

After obtaining the joint density $P(x, \theta)$ by maximizing the entropy, we can calculate the desired marginal $P(\theta) = \int dx P(x, \theta)$. The result is

$$P(\theta) = Q(\theta|x'), \quad (7)$$

where $Q(\theta|x') = \frac{Q(\theta)Q(x'|\theta)}{Q(x')}$ is the Bayes posterior $Q(\theta|x')$ given by Bayes theorem, which just follows from the rules of probability. This proves that maximum entropy as an inference engine justifies the usual Bayes procedure when the constraint is a datum such as knowing that a measurement of X turned out to give a value x' . Maximum entropy is used to show that Bayes theorem should be used in the inference process.

Going back to the EEG problem we consider that the relevant space is formed by the dipole variables at the two scales and the electrode potentials. Thus we seek the maximization of

$$S[P||Q] = - \int P(J_d, J_{d-1}, V) \log \frac{P(J_d, J_{d-1}, V)}{Q(J_d, J_{d-1}, V)} dJ_d dJ_{d-1} dV \quad (8)$$

to obtain $P(J_d, J_{d-1}, V)$, which in addition to normalization, is subject to

- (A) The marginal $P(V) = \delta(V - v')$, the measured data is v' .
- (B) $Q(J_{d-1})$ is given, e.g. by $\prod_{i \in \Lambda_{d-1}} f(J_{d-1, i} | \theta^{d-1}(r^{d-1}(i)))$ for some parametric family $f(J|\theta)$.
- (C) Knowledge about the process of renormalization is coded by $Q(J_d|J_{d-1})$ (see section 2.3.)
- Given J_d , knowledge of J_{d-1} is irrelevant for V : $Q(V|J_d J_{d-1}) = Q(V|J_d)$

Marginalization and the product rule of probability give

$$Q(J_d) = \int Q(J_{d-1}) Q(J_d|J_{d-1}) dJ_{d-1}. \quad (9)$$

which can be calculated from (B) and (C). Solving the maximization problem and taking the marginal of the maximum entropy distribution we obtain

$$P(J_d) = \frac{Q(J_d)Q(v'|J_d)}{Q(v')} \quad (10)$$

is given by what we would have expected, Bayes theorem, with the extra important ingredient brought in by equation 9, that the prior at this new scale is obtained by whatever information we have on J_{d-1} , i.e. $Q(J_{d-1})$ and the renormalization procedure $Q(J_d|J_{d-1})$.

If we wish to restrict the distributions to products of some parametric form, e.g. t-students, we have to use $Q(J_d|\hat{\alpha}_d^0, \gamma_d^0)$, from equation 9 given by

$$Q(J_d|\hat{\alpha}_d^0, \gamma_d^0) \approx \int Q(J_{d-1}|\hat{\alpha}_{d-1}^f, \gamma_{d-1}^f)Q(J_d|J_{d-1})dJ_{d-1}. \quad (11)$$

This is the backward renormalization step. The idea is to determine which distribution of J_d in the parametric space of the t-student distributions is closest to the integral on the right side of equation 11. So a posterior in the coarsest scale $d - 1$ induces a prior in the d scale. We can start at the lowest resolution with the same (α_0^i, γ_0^i) initial values at every site of the coarsest lattice Λ_0 , obtain via variational Bayes the parameters for the posterior of the J_0 from equation 10 and proceed for the next scales as represented by the map:

$$(\hat{\alpha}_{d-1}^f, \gamma_{d-1}^f) \xrightarrow{\text{BackRenorm}} (\hat{\alpha}_d^0, \gamma_d^0) \quad (12)$$

Beginning with a uniform prior at the coarsest scale, that is a set of parameters $(\hat{\alpha}_0^0, \gamma_0^0)$ uniform over the lattice Λ_0 , we iterate the mapping

$$(\hat{\alpha}_0^0, \gamma_0^0) \xrightarrow{\text{VB}} \dots \xrightarrow{\text{BackRenorm}} (\hat{\alpha}_d^0, \gamma_d^0) \xrightarrow{\text{VB}} (\hat{\alpha}_d^f, \gamma_d^f) \xrightarrow{\text{BackRenorm}} (\hat{\alpha}_{d+1}^0, \gamma_{d+1}^0) \xrightarrow{\text{VB}} \dots \quad (13)$$

to finally obtain a posterior at the finest scales described by $(\hat{\alpha}_D^f, \gamma_D^f)$, the desired answer to the inference problem.

Finally it must be emphasized that the marginal of the maximum entropy distribution $P(J_{d-1}) = \int P(J_d, J_{d-1}, V)dJ_d dV$ is given by Bayes theorem at the coarser level, $P(J_{d-1}) = Q(J_{d-1})Q(V'|J_{d-1}/Q(V'))$, showing that the new maximization of the entropy didn't alter the result obtained by the previous step. Reusing the same data within the realm of maximum entropy is not the same as naively reusing the data using just Bayes theorem updating. For ME it is harmless, as it imposes a constraint already satisfied, while for Bayes it represents the belief that the data were independently re-obtained, leading to a unwarranted decrease of uncertainty.

2.3 Backward renormalization priors

We now investigate the backward renormalization step given by equation 11. Renormalization is seldom a tidy business, and the fact that the dipoles are vectors and that the direction of their sum is not necessarily the same as the perpendicular to the surface of the cortex, does complicate things even further. The cortex is represented by triangular faces that are not in the same plane and thus the renormalized face is not simply related to the finner scale faces. Approximations are needed to advance and suggest a specific form for the mapping in display 12. Numerically we have investigated this suggestion and found some variations on the theme that lead to good results. We can analyze the backward renormalization in the following simplified context. Call $\lambda = |\Lambda_{d-1}|/|\Lambda_d|$ the ratio of degrees of freedom of a lattice at a stage $d - 1$ of renormalization, to the next, finner stage d . In this work $\lambda = 1/4$. When going from one lattice to a coarser one density variables are approximately renormalized according to a scaled block average:

$$J_{d-1}(j) = \lambda \sum_{i(j)} J_d(i) \quad (14)$$

where $i(j)$ means that the sum is over the set of degrees of freedom at $r^d(i)$ that are blocked to form the coarser degree of freedom at position $r^{d-1}(j)$. For independent $J_d(i)$ probability theory leads to the convolution

$$Q_{d-1}(J_{d-1}(j)) = \int \prod_{i(j)} [dJ_d(i)Q(J_d(i))] \delta \left(J_{d-1}(j) - \lambda \sum_{i(j)} J_d(i) \right).$$

Using the characteristic functions, $\Phi(k) = \mathcal{F}\mathcal{T}(Q(J))$, the Fourier transforms of the distributions:

$$\Phi_{d-1}(k) = [\Phi_d(\lambda k)]^{1/\lambda} \quad (15)$$

So the prior distribution of the dipole at the finer scale position i can be chosen by inverting a Fourier transform:

$$Q(J_d(i)) = \mathcal{I}\mathcal{F}\mathcal{T} \left([\Phi_{d-1}(\frac{k}{\lambda})]^\lambda \right) \quad (16)$$

For distributions stable under additions, this entails a simple backward renormalization of the distribution parameters.

From all this development, the main information we obtained is that the expected value of the precision of the gaussian prior of the dipole density should decrease at the new lattice in comparison with that of the posterior at the previous coarser lattice. For the more intricate renormalization we have to consider, a further improvement obtained numerically in the simulations is that not only the variance of the prior should be larger, but that at a given lattice the inferred position of a dipole might be a little off and seem to be at a neighboring site. Thus we introduced what we call *contamination*, by adding variance from the nearest and next nearest sites:

$$\frac{1}{\bar{\alpha}_{d+1}^{i(j),0}} = \frac{1}{\bar{\alpha}_d^{j,f}} + \frac{1}{3} \sum_{j_n} \frac{1}{\bar{\alpha}_d^{j_n,f}} + \frac{1}{9} \sum_{j_{nn}} \frac{1}{\bar{\alpha}_d^{j_{nn},f}}, \quad (17)$$

bringing in information from j , the parent site of i as well as the nearest neighbors (j_n) and the next nearest neighbors (j_{nn}) of j . This prevents early commitment of the position of a dipole. In the average, the precision scales as the backward renormalization step suggests. For all the sites i in the finer lattice Λ_d that give rise to a given renormalization block at $r^{d-1}(j)$, the prior of $J(r^d(i))$ will have renormalized parameters inherited from the block variable distribution of $J(r^{d-1}(j))$.

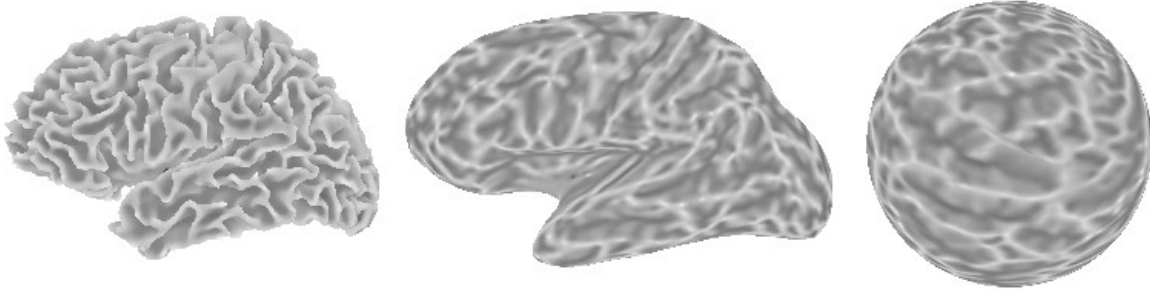


Figure 1: Cortex, left hemisphere (Left) original as obtained from a the structural MR image, (center) inflated, (right) spherical. Gray scale code the curvature in the original image.

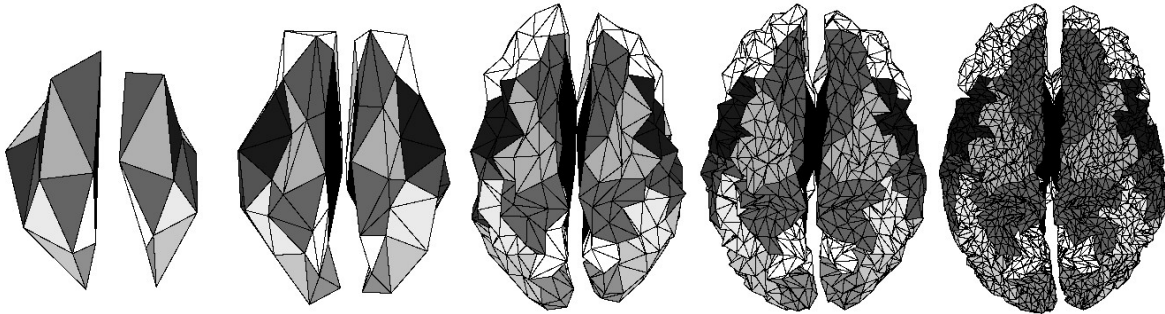


Figure 2: Representation of the cortex at different scales. Gray scale is used to represent finer scale balanced surfaces derived from the first representation, the icosahedral. The dipole density vectors are constrained to be at a site at the center and perpendicular to each triangular face.

3 Results and discussions

Depending on the choice of the initial and final renormalized lattice several methods can be defined. We denote them by $BRVB_{kk'}$, standing for Backward Renormalization Variational Bayes and k indicates the initial coarsest scale, k' the finest scale. The final lattice is obtained by five steps of renormalization. The full method is $BRVB_{04}$. The original Variational Bayes is VB, and since it runs at the finest scale only, and is the same as $BRVB_{44}$. We have also compared its performance to that of the MNE [11].

We first present results obtained by solving the inverse problem for artificial data generated by the forward problem, obtained by simulating two dipoles in the original lattice generated by Free Surfer. Manipulations include (i) the positions and magnitudes of the dipoles and (ii) noise corruption of the data. To quantify the quality of the inference we considered the distance between *real* and localized dipoles (defined in section 3.2) estimated by averaging over ≈ 200 runs.

Since studying the effect of adding noise to cases where $BRVB_{44}$ fails is not informative, we considered five different configurations where both algorithms performed equally well. Then, noise level was increased to study the decay of performance of the different methods.

We end by showing the results of applying the method to publicly available EEG data in a face recognition task (<http://www.fil.ion.ucl.ac.uk/spm/data/> SPM - Wellcome Trust Centre for Neuroimaging).

3.1 Simulations

We start by considering two main active dipoles in the original lattice at random positions $r(1)$ and $r(2)$, separated by a distance L ($55 \leq L \leq 65$ mm) from each other.

Each simulation starts at $t = 0$ runs for $T = 51$ samples, with each dipole intensity proportional to $\sin \frac{t\pi}{T}$. Results shown in the images comes from analysis made from data collected at the peak value $t = 26$.

The forward problem was solved using SPM (<http://www.fil.ion.ucl.ac.uk/spm/> - Wellcome Trust Centre for Neuroimaging) and Fieldtrip (<http://fieldtrip.fcdonders.nl/> - Centre for Cognitive Neuroimaging of the Donders Institute for Brain, Cognition and Behaviour) MATLAB toolboxes. They permit calculating the Lead Field using 3-spheres approximation (for simulations) and realistic head model BEM solutions (for analyses of real data). The Lead Field using 3-spheres was used to generate the potential in the head surface and the signal was then corrupted with NSR of 0.1. We used 128 electrodes positions and MRI template image available with the SPM toolbox. The inversion methods (MNE, BRVB₀₄ through BRVB₄₄) were implemented in MATLAB.

As described in section 2.2, each one of the 5 lattices $\Lambda_0, \dots, \Lambda_4$ has 40, 160, 640, 2560, 10240 faces, respectively. The dipoles are positioned using then mean of vertices and faces of the original lattice generated by Free Surfer. In the spherical surface, it is possible to localize the vertices and faces above each divided face (or the faces of the icosahedron for Λ_0). These original faces and vertices have their position in the original folded surface. Each dipole was located in the mean of those vertices and oriented as the mean of the normals of those faces. This could introduce localization bias since the density of faces in the original lattice is not homogeneous. The same set of lattices was generated using balanced representations, but the performance in all algorithms did not change (results not reported for brevity), so this option was discarded. For more information see [12].

Figure 3 shows as an example a particular run. In the first line, first panel in the left, the *real* dipole sources used to generate the data V . The following panels shows the estimated sources using Minimum Norm or MNE, BRVB₀₄ and BRVB₄₄, respectively. Figure 4 shows the variance or inverse precision $1/\alpha_n$ initial value in the two first columns and after convergence in the two last columns, at each scale for BRVB₀₄ in the first 5 lines and in the single grid BRVB₄₄ in the last.

This is a nice example to show because it exemplifies the case when the random choice of the location of the sources placed one on a deep position, which is known to present a problem since the Lead field is very small. This problem has been addressed by [20] using the precision matrix, but here this information is extracted from the data. While the BRVB₄₄ found only one, the more superficial source, the BRVB₀₄ was able to find both sources. For the two source case, about 10% of the 100 runs analyzed showed this difference in the behavior for deep sources and the method was seen to be robust under this condition.

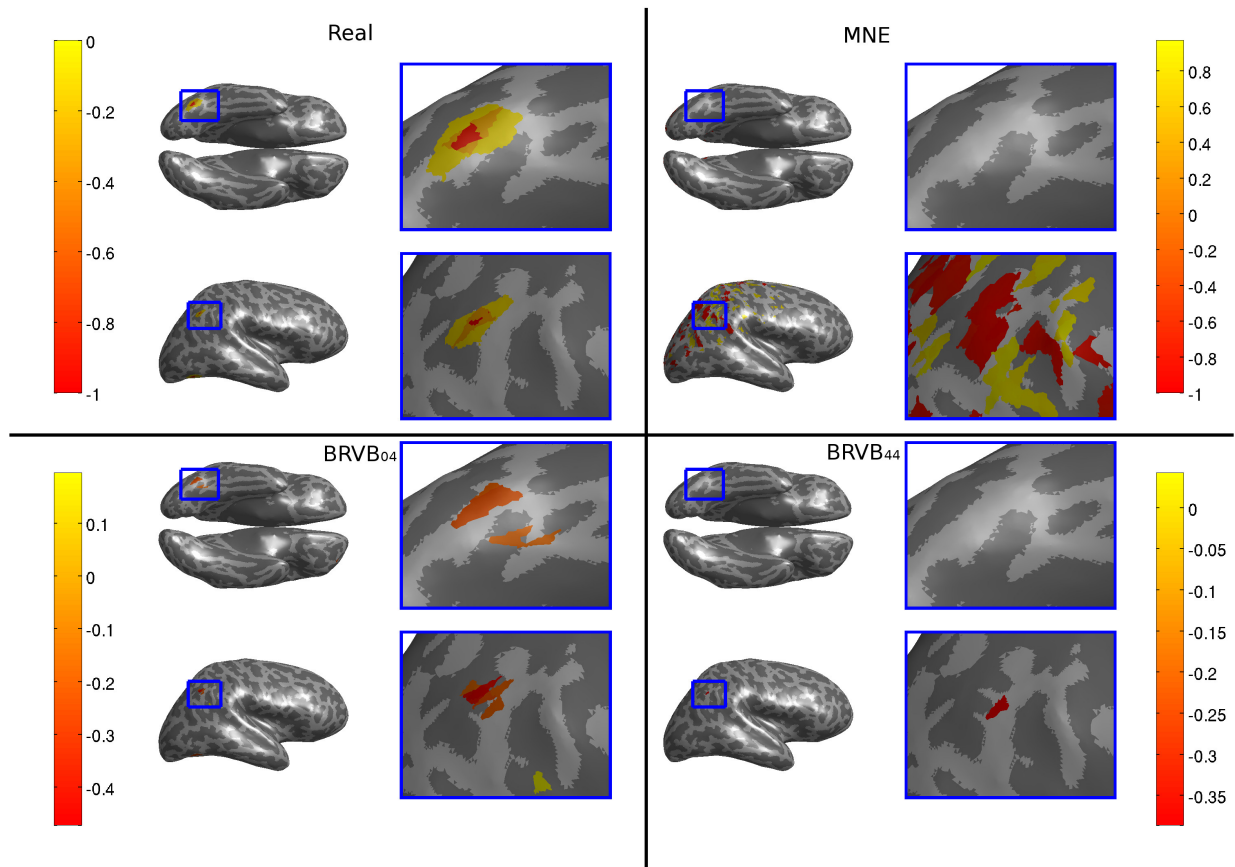


Figure 3: The top left box represents the real current densities used to simulate the potential, while the others represents the different localization methods. Top and bottom line of each box represents the bottom and right view of the inflated cortex facing right, respectively. The first column represents the partially inflated brain and the second zooms into the indicated region. Color codes the current intensity, negative facing inwards and positive outwards. The cortex is represented by a lattice of $\approx 2.8 \times 10^4$ triangles and the fifth order grid is made up by $10240 = 2 \times 20 \times 4^4$ possible dipole locations.

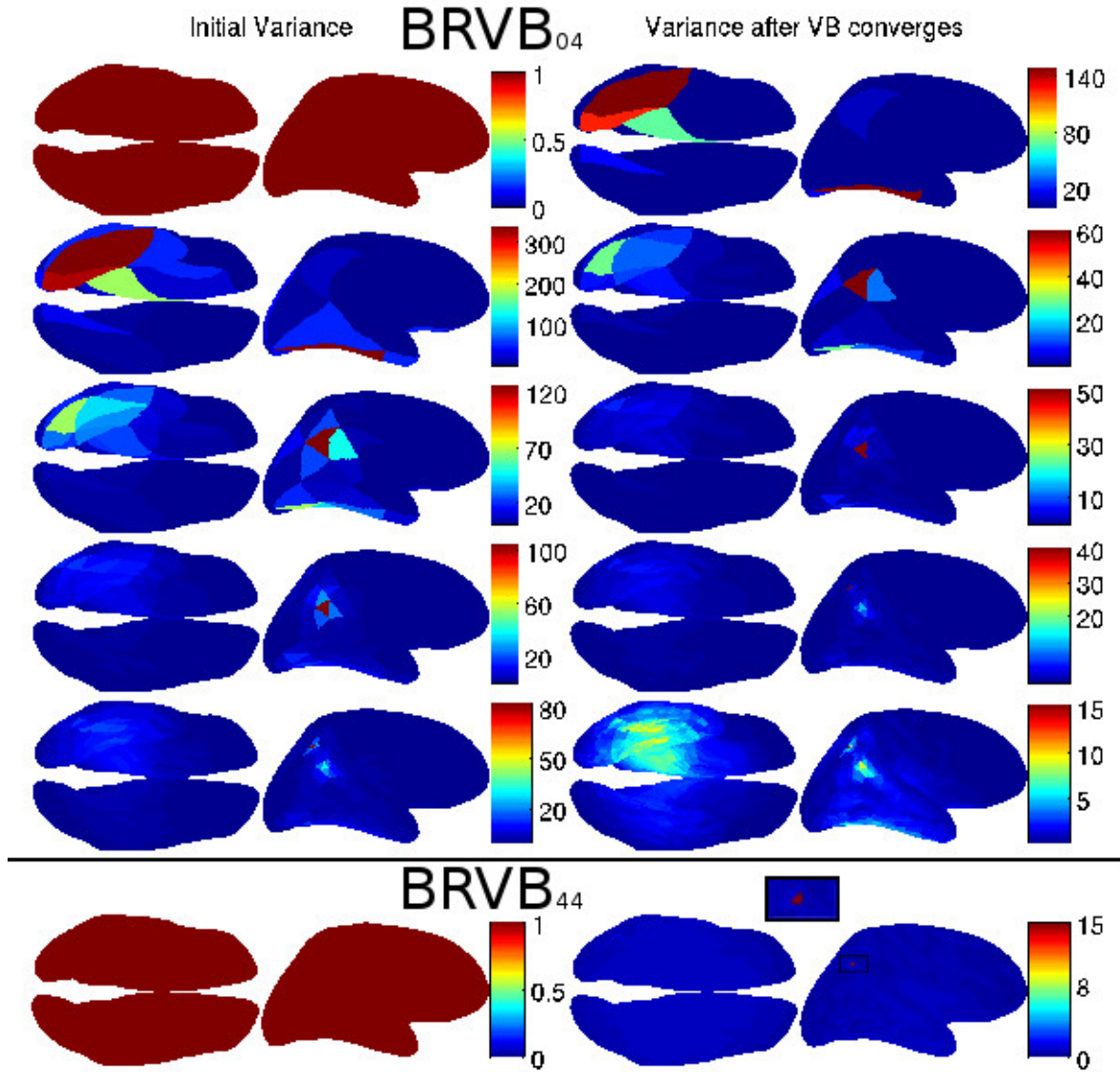


Figure 4: Evolution of $1/\alpha$ under iteration of the backward renormalization algorithm. First and third columns shows the bottom view of the cortex surface, while second and fourth columns shows the right hemisphere, both facing right. First and second columns shows initial variance in each region, while third and fourth columns shows variance after the VB algorithm converged in that specific grid, with a given initial value. First to fifth rows show the stages of BRVB algorithm in each grid with: first $BRVB_{00}$ ($40 = 2 \times 20$ faces), second $BRVB_{01}$ (160) third $BRVB_{02}$ (640), fourth $BRVB_{03}$ (2560) and fifth $BRVB_{04}$ (10240) ($2 \times 20 \times 4^d$ faces). The last line is the variance in the VB algorithm starting with a hyperparameter $\bar{\alpha}$ uniform in the fifth lattice, $BRVB_{44}$. Notice how aggressive is the convergence in the variance when the VB method starts with a uniform prior in the last surface, as evidenced by the zoomed square.

3.2 Validation of the method

The main reason for simulating this problem is that it allows for comparisons with the *real* sources, used to generate the data. We used mainly the distance between the strongest and second strongest localized dipoles.

To begin we compare the distances in mm between *real* and localized dipoles in the 200 simulations. As we can see in Figure 5, we first compare the strongest dipole found by the methods $BRVB_{44}$ and $BRVB_{04}$ and the strongest *real* dipole. We also compare it to the minimum between the distances of the first and second strongest localized ones, ignoring differences in amplitudes. It is interesting to see that even in this case there is a peak at 60 mm, specially for the $BRVB_{44}$.

Finally we show the ordered errors for all simulations, from $BRVB_{44}$ to $BRVB_{04}$, evidencing the improvement in the use of each additional localization.

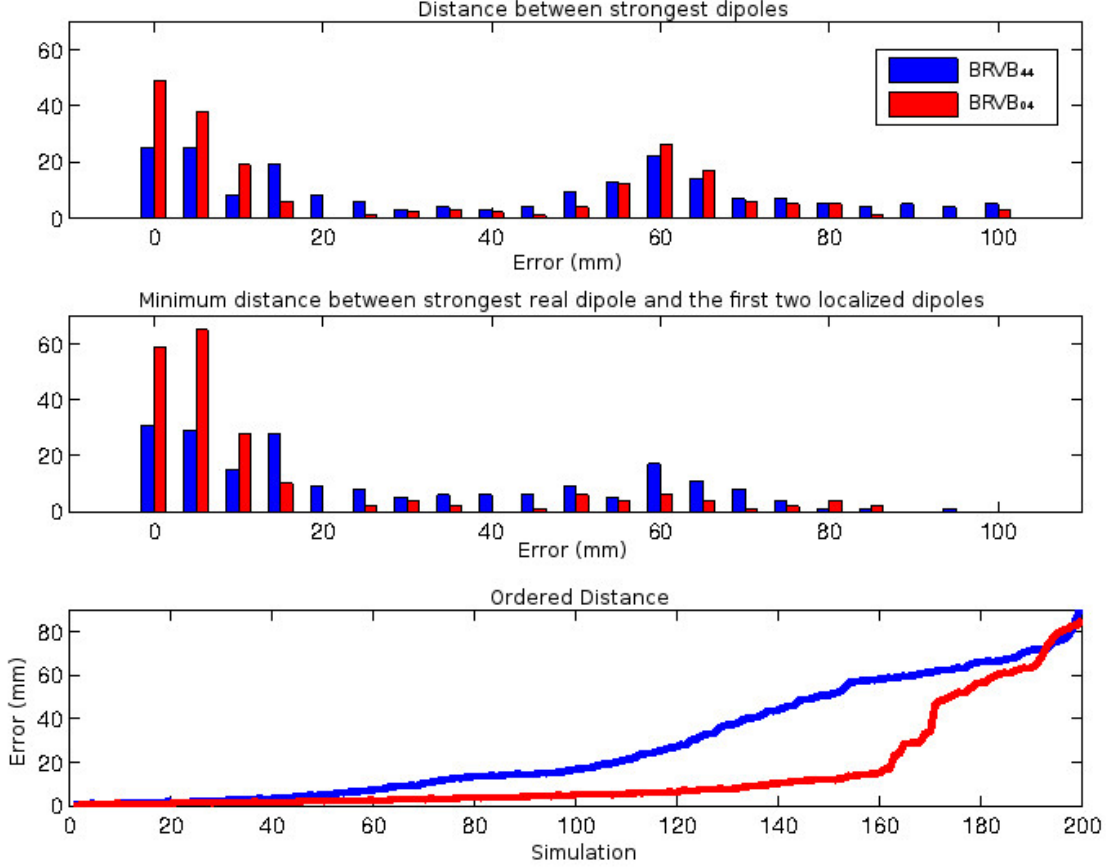


Figure 5: First line shows the histograms for the distance (mm) between the strongest *real* source and that found by different algorithms: BRVB₀₄ and BRVB₄₄. Second line is the same type of histogram but showing the smallest distance between the strongest *real* source and the two strongest localized dipoles. This way, since we used two sources for generating the field, we don't care which one was localized as the strongest, only its position. The last line shows the same information as the second histogram, but ordering the errors in ascendant fashion. Obtained from inference made on 200 different forward problems, with random positions and distances between the two dipoles randomly chosen between 55 and 65 mm.

We also analyzed how different algorithms fare under the addition of different levels of noise.

We identified 5 simulations where both the BRVB₄₄, BRVB₃₄ and BRVB₀₄ obtained similar good results from data corrupted at low noise-to-signal ratios (NSR=0.1). In order to compare runs with similar good results, we have to restrict to cases where the sources are located in more superficial regions, since the performance for sources in deep locations are quite different with the single scale method not even identifying a result to be compared. We added uncorrelated gaussian noise of zero mean and variance σ^2 to each of the M components (electrodes) of the vector V of data voltages so that

$$NSR = \frac{M \sigma^2}{V'V}. \quad (18)$$

Finally, in Figure 6, besides the error distance in localization, we also plotted the ROC space for the three algorithms, and the curves for the distance between the average false pos-

itives positions to the *real* dipoles. Notice how the the $BRVB_{04}$ has a clear superior resistance to the increased noise.

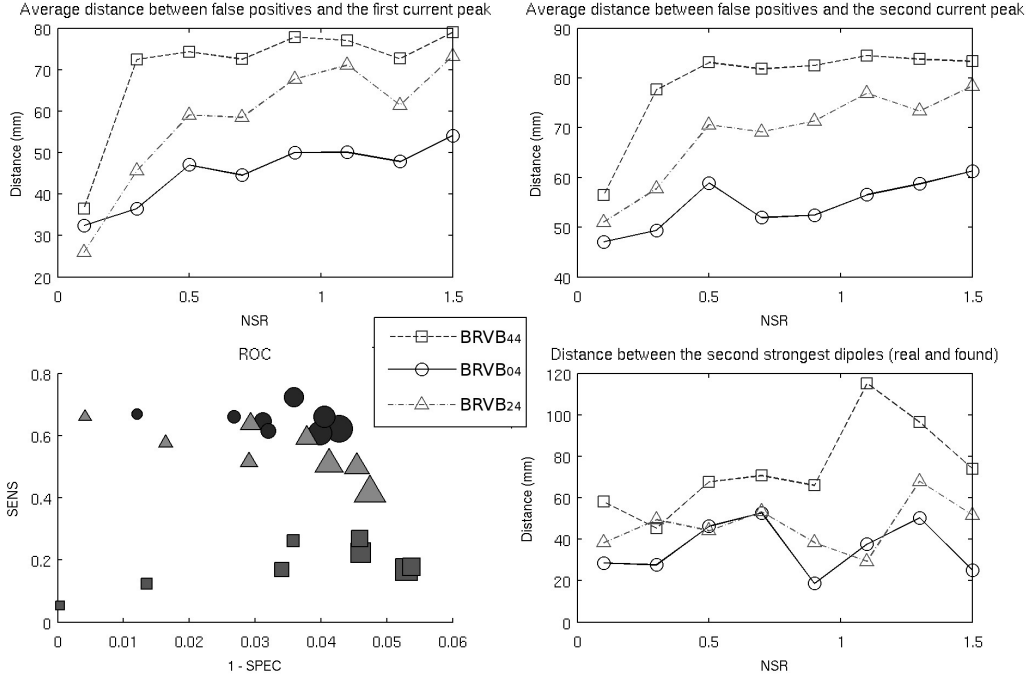


Figure 6: Performance of the different algorithms. The horizontal axis represents the noise to signal ratio (apart from the ROC space). First line : average distance between false positives and the most intense real dipole on the left, and the second most intense on the right. Second line : ROC space on the left (the size of the markers represents the intensity of noise), and average distance between the second most intense true positive and the second most intense real dipole on the right.

3.3 Real Data from EEG

We applied the $BRVB_{04}$ and the $BRVB_{44}$ in real data available at <http://www.fil.ion.ucl.ac.uk/spm/data/mmfaces/> (SPM - Wellcome Trust Centre for Neuroimaging). The experiment consists of 128 electrodes set in a Face / No-Face stimulus. We preprocessed the data as specified in the tutorial for source reconstruction in SPM, and computed the difference between the average of each condition. The resulting scalp potential was used for the source localization. The sources shown in Figure 7 were found by $BRVB_{04}$, $BRVB_{44}$ and MNE. Although they are in general consistent with the literature for this experiment [10], the location of the sources as well the intensity is clearly different. Further studies are necessary to understand the nature of this difference in this specific protocol.

4 Conclusion

The main contribution of this paper is to use a Maximum Entropy inferential chain of projections to systematically transfer posterior information from one coarse scale to the prior of a finer scale. This approach is not restricted to M/EEG or fMRI imaging methods, but should apply to inference about the localization of sources in any spatially extended system and thus has a potentially wide scope of applications. We analyzed the behavior of the hierarchical Bayesian approach for solving the M/EEG inverse problem. This was introduced into this context by [22] who used one coarser grid to restrict the search in a finer scale, without propagating the converged variance to the next scale. As shown by Nummenmaa *et al* [16], the Variational Bayes approach is very sensitive to the initial values of the hyperparameters.

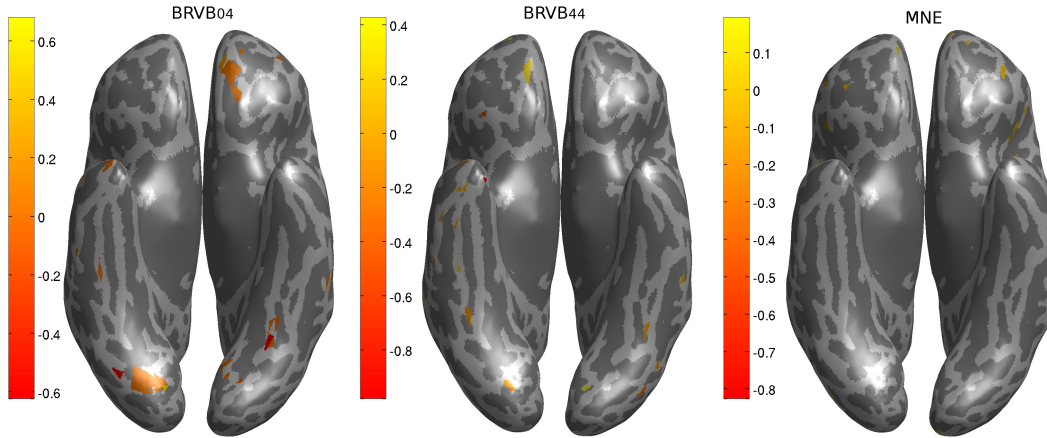


Figure 7: Bottom view of the cortex looking up (most significant locations are on the bottom in that instant). From left to right : $BRVB_{04}$, $BRVB_{44}$ and MNE at approximately 170 ms.

Our multiscale approach was inspired by the fMRI work of [1] to systematically construct prior distributions. An important difference is that the M/EEG data introduces a further complication by not being a scalar as in the fMRI case, leading us to defining *a priori* directions for the dipoles, or risk having to deal with a nonlinear problem with a too large number of degrees of freedom. This simplicity permitted the more sophisticated formulation based on the backward renormalization group for discrete variables done in [4]. Our method permits setting the initial value for the hyperparameters in the VB approach on a finer scale from the value obtained after VB convergence in the coarser previous scale. The method being robust to choices in the coarsest scale. However the renormalization group analysis of this harder problems remains incomplete and further work in this direction will follow.

Second, we have done extensive simulations to validate the method. We presented results in simulated data that suggests that this approach is a valid aid to increase the precision of the localized dipoles and also to increase the performance in the presence of noise. The backward renormalization priors permitted a more systematic localization of deep sources far from the skull.

Third, as mentioned by Nummenmaa *et al* [16] in the discussion, there appears to be a natural trade-off between choosing a method providing smoother but unique solution, and the hierarchical approach with better spatial resolution and a multitude of candidate solutions. We claim that our method might represent a good direction in finding a compromise between both solutions.

We stress that the main advantages of a Maximum Entropy or Bayesian approach is the clear identification of the often hidden assumptions underlying an algorithmic approach. This permits concentrating on the different pieces needed to solve the puzzle. It illustrates the fact that prior information not only goes into the prior but can improve the likelihood. While we need a better electromagnetic model of the brain as well as understanding the noise processes, here we just looked at the prior, but this can certainly be improved. A natural idea is to improve our method with anatomical prior information as used by [19].

Acknowledgements We thank Ariel Caticha, Selene Amaral and Said Rabbani for discussions on different aspects of inference and neuroimaging. This work received support from CNAIPS-USP and CNPq.

References

- [1] Amaral, R., Rabbani, S. R., and Caticha, N. (2004). Multigrid priors for a Bayesian approach to fMRI. *NeuroImage*, 23:654 – 662.
- [2] Amaral, R., Rabbani, S. R., and Caticha, N. (2006). BOLD response analysis by iterated local multigrid priors. *NeuroImage*, 36:361 – 369.
- [3] Bishop, C. M. (2007). *Pattern Recognition and Machine Learning (Information Science and Statistics)*. Springer, 1 edition.
- [4] Caticha, N. (2015). Source localization by entropic inference and backward renormalization group priors. *Entropy*, submitted.
- [5] Dale, A. M. and Sereno, M. I. (1993). Improved Localization of Cortical Activity by Combining EEG and MEG with MRI Cortical Surface Reconstruction: A Linear Approach. *Journal of Cognitive Neuroscience*, 5:162–176.
- [6] Fischl, B., Sereno, M. I., and Dale, A. M. (1999a). Cortical surface-based analysis. I. Segmentation and Surface Reconstruction. *NeuroImage*, 9(2):195–207.
- [7] Fischl, B., Sereno, M. I., and Dale, a. M. (1999b). Cortical surface-based analysis. II: Inflation, flattening, and a surface-based coordinate system. *NeuroImage*, 9(2):195–207.
- [8] Geselowitz, D. (1967). On Bioelectric Potentials in an Inhomogeneous Volume Conductor. *Biophysical Journal*, 7(1):1–11.
- [9] Giffin, A. and Caticha, A. (2007). Updating probabilities with data and moments. *Bayesian Inference and Maximum Entropy Methods in Science and Engineering, AIP Conf. Proc, Ed. A. Mohammad-Djafari*, 872:31.
- [10] Halgren, E. (2000). Cognitive Response Profile of the Human Fusiform Face Area as Determined by MEG. *Cerebral Cortex*, 10(1):69–81.
- [11] Hamalainen, M. and Ilmoniemi, R. (1994). Interpreting magnetic fields of the brain: minimum norm estimates. *Medical and Biological Engineering and Computing*, 32:35–42. 10.1007/BF02512476.
- [12] Lin, F.-H., Belliveau, J. W., Dale, A. M., and Hämäläinen, M. S. (2006). Distributed current estimates using cortical orientation constraints. *Human brain mapping*, 27(1):1–13.
- [13] Mosher, J. C., Leahy, R. M., and Lewis, P. S. (1999). EEG and MEG: forward solutions for inverse methods. *IEEE transactions on bio-medical engineering*, 46(3):245–59.
- [14] Mosher, J. C., Lewis, P. S., and Leahy, R. M. (1992). Multiple dipole modeling and localization from spatio-temporal MEG data. *IEEE transactions on bio-medical engineering*, 39(6):541–57.
- [15] Neal, R. M. (1997). Bayesian Learning for Neural Networks (Lecture Notes in Statistical Vol. 118). *Journal of the American Statistical Association*, 92(438):791.

- [16] Nummenmaa, A., Auranen, T., Hämäläinen, M. S., Jääskeläinen, I. P., Lampinen, J., Sams, M., and Vehtari, A. (2007). Hierarchical Bayesian estimates of distributed MEG sources: theoretical aspects and comparison of variational and MCMC methods. *NeuroImage*, 35(2):669–85.
- [17] Nunez, P. L. and Srinivasan, R. (2006). *Electric Fields of the Brain: The Neurophysics of EEG, 2nd Edition*. Oxford University Press.
- [18] Oostendorp, T. F. and van Oosterom, a. (1989). Source parameter estimation in inhomogeneous volume conductors of arbitrary shape. *IEEE transactions on bio-medical engineering*, 36(3):382–91.
- [19] Ou, W., Nummenmaa, A., Ahveninen, J., Belliveau, J. W., Hämäläinen, M. S., and Golland, P. (2010). NeuroImage Multimodal functional imaging using fMRI-informed regional EEG / MEG source estimation. *NeuroImage*, 52(1):97–108.
- [20] Pascual-Marqui, R. D. (2002). Standardized low-resolution brain electromagnetic tomography (sLORETA): technical details. *Methods and findings in experimental and clinical pharmacology*, 24 Suppl D:5–12.
- [21] Ramirez, R. R. (2008). Source localization. *Scholarpedia*, 3(11):1733.
- [22] Sato, M.-a., Yoshioka, T., Kajihara, S., Toyama, K., Goda, N., Doya, K., and Kawato, M. (2004). Hierarchical bayesian estimation for meg inverse problem. *NeuroImage*, 23(3):806–826.
- [23] Scharf, G. and Scharf, C. (2010). Electrophysiology of living organs from first principles. page 11.
- [24] Wipf, D. and Nagarajan, S. (2009). A unified Bayesian framework for MEG / EEG source imaging. *NeuroImage*, 44(3):947–966.